

# LUXendins reveal endogenous glucagon-like peptide-1 receptor distribution and dynamics

Julia Ast<sup>1,2</sup>, Anastasia Arvaniti<sup>1,2</sup>, Nicholas H.F. Fine<sup>1,2</sup>, Daniela Nasteska<sup>1,2</sup>, Fiona B. Ashford<sup>1,2</sup>, Zania Stamatakis<sup>3</sup>, Zsombor Koszegi<sup>1,2</sup>, Andrea Bacon<sup>4</sup>, Stefan Trapp<sup>5</sup>, Ben J. Jones<sup>6</sup>, Benoit Hastoy<sup>7</sup>, Alejandra Tomas<sup>8</sup>, Christopher A. Reissaus<sup>9</sup>, Amelia K. Linnemann<sup>9</sup>, Elisa D'Este<sup>10</sup>, Davide Calebiro<sup>1,2</sup>, Kai Johnsson<sup>11</sup>, Tom Podewin<sup>11\*</sup>, Johannes Broichhagen<sup>11\*</sup> and David J. Hodson<sup>1,2\*</sup>

<sup>1</sup> Institute of Metabolism and Systems Research (IMSR), and Centre of Membrane Proteins and Receptors (COMPARE), University of Birmingham, Birmingham, UK.

<sup>2</sup> Centre for Endocrinology, Diabetes and Metabolism, Birmingham Health Partners, Birmingham, UK.

<sup>3</sup> Centre for Liver Research, College of Medical and Dental Sciences, Institute for Immunology and Immunotherapy, University of Birmingham, Birmingham, UK.

<sup>4</sup> Genome Editing Facility, Technology Hub, University of Birmingham, Birmingham, UK.

<sup>5</sup> Centre for Cardiovascular and Metabolic Neuroscience, Department of Neuroscience, Physiology & Pharmacology, University College London, London, UK

<sup>6</sup> Imperial College London, Section of Investigative Medicine, Division of Diabetes, Endocrinology and Metabolism, London, UK.

<sup>7</sup> Oxford Centre for Diabetes, Endocrinology & Metabolism, University of Oxford, Oxford, UK

<sup>8</sup> Imperial College London, Section of Cell Biology and Functional Genomics, Division of Diabetes, Endocrinology and Metabolism, London, UK.

<sup>9</sup> Department of Pediatrics, Indiana University School of Medicine, Indianapolis, IN, USA.

<sup>10</sup> Optical Microscopy Facility, Max Planck Institute for Medical Research, Heidelberg, Germany.

<sup>11</sup> Department of Chemical Biology, Max Planck Institute for Medical Research, Heidelberg, Germany.

\*Correspondence should be addressed to: [d.hodson@bham.ac.uk](mailto:d.hodson@bham.ac.uk),  
[johannes.broichhagen@mpimf-heidelberg.mpg.de](mailto:johannes.broichhagen@mpimf-heidelberg.mpg.de) or [tom.podewin@mpimf-heidelberg.mpg.de](mailto:tom.podewin@mpimf-heidelberg.mpg.de)

**Keywords:** incretin, diabetes, beta cell, alpha cell, fluorescent probes, CRISPR, nanoscopy.

**Word count:** 3534 (excluding Abstract, Methods, References and Legends).

43 **ABSTRACT** (150 words)

44 The glucagon-like peptide-1 receptor (GLP1R) is a class B G protein-coupled receptor  
45 (GPCR) involved in metabolism. Presently, its visualization is limited to genetic manipulation,  
46 antibody detection or the use of probes that stimulate receptor activation. Herein, we present  
47 **LUXendin645**, a far-red fluorescent GLP1R antagonistic peptide label. **LUXendin645**  
48 produces intense and specific membrane labeling throughout live and fixed tissue. GLP1R  
49 signaling can additionally be evoked when the receptor is allosterically modulated in the  
50 presence of **LUXendin645**. Using **LUXendin645** and STED-compatible **LUXendin651** we  
51 describe islet GLP1R expression patterns, reveal higher-order GLP1R organization including  
52 the existence of membrane nanodomains, and track single receptor subpopulations. We  
53 furthermore show that different fluorophores can confer agonistic behavior on the **LUXendin**  
54 backbone, with implications for the design of stabilized incretin-mimetics. Thus, our labeling  
55 probes possess divergent activation modes, allow visualization of endogenous GLP1R, and  
56 provide new insight into class B GPCR distribution and dynamics.

57

## 58 INTRODUCTION

59 The glucagon-like peptide-1 receptor (GLP1R) is a secretin family class B G protein-coupled  
60 receptor (GPCR) characterized by hormone regulation.<sup>1</sup> Due to its involvement in glucose  
61 homeostasis, the GLP1R has become a blockbuster target for the treatment of type 2  
62 diabetes mellitus.<sup>2</sup> The endogenous ligand, glucagon-like peptide-1 (GLP-1) is released from  
63 enteroendocrine L-cells in the gut in response to food intake,<sup>3</sup> from where it travels to the  
64 pancreas before binding to its cognate receptor expressed in  $\beta$ -cells. Following activation,  
65 the GLP1R engages a cascade of signaling pathways including  $\text{Ca}^{2+}$ , cAMP, ERK and  $\beta$ -  
66 arrestin, which ultimately converge on  $\beta$ -cell survival and the glucose-dependent  
67 amplification of insulin release.<sup>4,5</sup> GLP1R is also expressed in the brain<sup>6</sup> and muscle<sup>7</sup> where  
68 it further contributes to metabolism *via* effects on food intake, energy expenditure,  
69 locomotion and insulin sensitivity. Despite this, GLP1R localization remains a challenge and  
70 is impeding functional characterization of GLP-1 and drug action.

71 Chemical biology and recombinant genetics have made available a diverse range of  
72 methods for the visualization of biological entities. Thus, classical fluorescent protein-  
73 fusions,<sup>8</sup> self-labeling suicide enzymes (SNAP-, CLIP-, and Halo-tag),<sup>9-11</sup> “click  
74 chemistry”<sup>12,13</sup> and fluorogenic probes<sup>14-16</sup> have provided unprecedented insight into the  
75 localization and distribution of their respective targets in living cells. In particular, current  
76 approaches for visualizing the GLP1R have so far relied on monoclonal antibodies (mAbs)  
77 directed against GLP1R epitopes,<sup>17,18</sup> or fluorescent analogues of Exendin4(1-39),<sup>19-21</sup> a  
78 stabilized form of GLP-1 and the basis for the incretin-mimetic class of drugs. Moreover,  
79 floxed mouse models exist in which Cre recombinase is driven by the *Glp1r* promoter,  
80 allowing labeling of GLP1R-expressing cells when crossed with reporter mice.<sup>6,7</sup>

81 Such methods have a number of shortcomings. Antibodies possess variable specificity<sup>18</sup> and  
82 tissue penetration, and GLP1R epitopes might be hidden or preferentially affected by fixation  
83 in different cell types. Even more, fluorescent analogues of Exendin4(1-39) activate and  
84 internalize the receptor, which could confound results in live cells, particularly when used as  
85 a tool to sort purified populations (*i.e.*  $\beta$ -cells) for transcriptomic analysis.<sup>22,23</sup> On the other  
86 hand, reporter mouse strategies possess high fidelity, but cannot account for post-  
87 translational processing, protein stability and trafficking of native receptor.<sup>24</sup> Lastly, none of  
88 the aforementioned approaches are amenable to super-resolution imaging of GLP1R.

89 Given the wider reported roles of GLP-1 signaling in the heart,<sup>25</sup> liver,<sup>26</sup> immune system<sup>2</sup> and  
90 brain,<sup>27</sup> it is clear that new tools are urgently required to help identify GLP-1 target sites, with  
91 repercussions for drug treatment and its side effects. In the present study, we therefore set  
92 out to generate a specific probe for endogenous GLP1R detection in its native, surface-  
93 exposed state in live and fixed tissue, without receptor activation. Herein, we report  
94 **LUXendin645** and **LUXendin651**, Cy5- and SiR- conjugated far-red fluorescent antagonists  
95 with unprecedented specificity, live tissue penetration and super-resolution capability. Using  
96 our tools, we provide an updated view of GLP1R expression patterns in the islet of  
97 Langerhans, show that endogenous GLP1Rs form nanodomains at the membrane and  
98 reveal receptor subpopulations with distinct diffusion modes. Lastly, we find that installation  
99 of a TMR fluorophore unexpectedly confers potent agonist properties. As such, the  
100 **LUXendins** provide the first nanoscopic characterization of a class B GPCR, with wider  
101 flexibility for detection and interrogation of GLP1R in the tissue setting.

## 102 RESULTS

### 103 Design and synthesis of LUXendin555, LUXendin651 and LUXendin645

104 Ideally, a fluorescent probe to specifically visualize a biomolecule should have the following  
105 characteristics: straightforward synthesis and easy accessibility, high solubility, relative small  
106 size, high specificity and affinity, and a fluorescent moiety that exhibits photostability,  
107 brightness, (far-)red fluorescence with an additional two-photon cross-section. Moreover, the  
108 probe should be devoid of biological effects when applied to live cells and show good or no  
109 cell permeability, depending on its target localization. While some of these points were  
110 addressed in the past (*vide infra*), we set out to achieve this high bar by designing a highly  
111 specific fluorescent GLP1R antagonist using TMR, Cy5 and SiR fluorophores. As no small  
112 molecule antagonists for the GLP1R are known, we turned to Exendin4(9-39), a potent  
113 antagonistic scaffold amenable to modification (Fig. 1).<sup>28</sup> We used solid-phase peptide  
114 synthesis (SPPS) to generate an S39C mutant,<sup>29</sup> which provides a C-terminal thiol handle  
115 for late-stage installation of different fluorophores. As such, TMR-, Cy5- and SiR-conjugated  
116 versions were obtained by means of cysteine-maleimide chemistry, termed **LUXendin555**,  
117 **LUXendin645**, and **LUXendin651**, respectively (spectral properties are shown in Table 1,  
118 HPLC traces and HRMS characterization can be found in the SI) (Fig. 1).

119 **Table 1: Spectral properties of GLP1R labeling probes.** Maximal excitation and emission  
120 wavelengths, and quantum yields were acquired using probes dissolved at 10  $\mu\text{M}$  in PBS, pH  
121 7.4 at 21 °C.

	dye	$\lambda_{\text{Ex}} / \text{nm}$	$\lambda_{\text{Em}} / \text{nm}$	$\epsilon^{[\text{a}]} / \text{M}^{-1} \text{cm}^{-1}$	$\Phi$
<b>LUXendin555</b>	TMR	555	579	84,000	0.31
<b>LUXendin645</b>	Cy5	645	664	250,000	0.22
<b>LUXendin651</b>	SiR	651	669	100,000	0.43

122 <sup>[a]</sup> For maleimide-conjugated fluorophores

123

### 124 LUXendin645 intensely labels GLP1R in cells and tissue

125 GLP-1-induced cAMP production ( $EC_{50}(\text{cAMP}) = 2.8 \text{ nM}$ , 95% CI [1.5-5.2]) was similarly  
126 blocked by Exendin4(9-39) ( $EC_{50}(\text{cAMP}) = 38.4 \text{ nM}$ , 95% CI [19.0-77.8]) and its S39C  
127 mutant ( $EC_{50}(\text{cAMP}) = 34.8 \text{ nM}$ , 95% CI [18.8-64.4]) (Fig. 2a). Installation of Cy5 to produce  
128 **LUXendin645** did not affect these antagonist properties ( $EC_{50}(\text{cAMP}) = 73.1 \text{ nM}$ , 95% CI  
129 [54.9-97.5]) (Fig. 2a). As expected, addition of the GLP1R positive allosteric modulator  
130 (PAM) BETP<sup>30</sup> conferred agonist activity on **LUXendin645** ( $EC_{50}(\text{cAMP}) = 9.3 \text{ nM}$ , 95% CI  
131 [2.2-40.0]), with a potency similar to Exendin4(1-39) ( $EC_{50}(\text{cAMP}) = 18.3 \text{ nM}$ , 95% CI [8.0-  
132 42.1]) (Fig. 2b).

133 As a first assessment of GLP1R labeling efficiency, we probed YFP-AD293-SNAP\_GLP1R  
134 cells with increasing concentrations of **LUXendin645**. Maximum labeling occurred at 100 nM  
135 (Fig. 2c), in good agreement with the previously published  $K_d = 15.8 \text{ nM}$  of native  
136 Exendin4(9-39)<sup>31</sup>. **LUXendin645** was unable to label YFP-AD293 cells in which the GLP1R  
137 was absent (Fig. 2d).

138 We next examined whether **LUXendin645** would allow labeling of endogenous GLP1R.  
139 Following 60 min application of 50 nM **LUXendin645**, isolated islets demonstrated intense  
140 and clean labeling, which was restricted to the membrane (Fig. 2e). Using conventional

141 confocal microscopy, we were able to detect bright staining even 60  $\mu\text{m}$  into the islet (Fig.  
142 2e). Given these results, we next attempted to penetrate deeper into the islet by taking  
143 advantage of the superior axial resolution of two-photon excitation (Fig. 2f). Remarkably, this  
144 imaging modality revealed **LUXendin645** labeling at high resolution throughout the entire  
145 volume of the islet (170  $\mu\text{m}$  in this case) (Fig. 2f). Consistent with the cAMP assays,  
146 profound GLP1R internalization was detected following co-application of **LUXendin645** and  
147 BETP to MIN6  $\beta$ -cells, which endogenously express the receptor (Fig. 2g, h).

#### 148 **LUXendin645 allows multiplexed GLP1R detection**

149 Demonstrating flexibility, **LUXendin645** labeling was still present following formaldehyde  
150 fixation (Fig. 2i, j). Immunostaining using a specific primary monoclonal antibody against the  
151 GLP1R revealed strong co-localization with **LUXendin645** in both islets (Fig. 2i) and MIN6  
152 cells (Fig. 2j). Notably, **LUXendin645** displayed superior signal-to-noise-ratio and membrane  
153 resolution compared to the antibody (Fig. 2k), expected to be even better in live tissue where  
154 auto-fluorescence is less. Likewise, **LUXendin645** co-localized with SNAP-Surface 488 in  
155 SNAP\_GLP1R-INS1 rat  $\beta$ -cells generated on an endogenous null background (Fig. 2l).  
156 Suggesting that **LUXendin645** requires the presence of surface GLP1R, labeling was  
157 markedly reduced following prior internalization with Exendin4(1-39) (Fig. 2l, m).

#### 158 **LUXendin645 specifically binds the GLP1R**

159 To further validate the specificity of **LUXendin645** labeling in primary tissue, we generated  
160 *Glp1r* knock-out mice. This was achieved using CRISPR-Cas9 genome editing to introduce  
161 a deletion into exon 1 of the *Glp1r*. The consequent frameshift was associated with absence  
162 of translation and therefore a global GLP1R knockout, termed *Glp1r*<sup>(GE)-/-</sup>, in which all intronic  
163 regions, and thus regulatory elements, are preserved (Fig. 3a, b). Wild-type (*Glp1r*<sup>+/+</sup>),  
164 heterozygous and homozygous littermates were phenotypically normal and possessed  
165 similar body weights (Fig. 3c).

166 Confirming successful GLP1R knock-out, insulin secretion assays in islets isolated from  
167 *Glp1r*<sup>(GE)-/-</sup> mice showed intact responses to glucose, but absence of Exendin4(1-39)-  
168 stimulated insulin secretion (Fig. 3d). Reflecting this finding, the incretin-mimetic Liraglutide  
169 was only able to stimulate cAMP rises in islets from wild-type (*Glp1r*<sup>+/+</sup>) littermates,  
170 measured using the FRET probe Epac2-camps (Fig. 3e, f). As expected, immunostaining  
171 with monoclonal antibody showed complete absence of GLP1R protein (Fig. 3g). Suggesting  
172 that **LUXendin645** specifically targets GLP1R, with little to no cross-talk from glucagon-  
173 receptors,<sup>32</sup> signal could not be detected in *Glp1r*<sup>(GE)-/-</sup> islets (Fig. 3g).

174 Together, these data provide strong evidence for a specific mode of **LUXendin645** action  
175 via the GLP1R.

#### 176 **LUXendin645 highlights weak GLP1R expression**

177 Previous approaches have shown low abundance of *Glp1r* transcripts in the other major islet  
178 endocrine cell type, *i.e.* glucagon-secreting  $\alpha$ -cells.<sup>7,33</sup> This is associated with detection of  
179 GLP1R protein in ~1-10% of cells,<sup>7,34</sup> providing an excellent testbed for **LUXendin645**  
180 sensitivity. Studies in intact islets showed that **LUXendin645** labeling was widespread in the  
181 islet and well co-localized with insulin immunostaining (Fig. 4a). However, **LUXendin645**  
182 could also be seen on membranes very closely associated with  $\alpha$ -cells and somatostatin-

183 secreting  $\delta$ -cells (Fig. 4b, c), similarly to results obtained with GLP1R mAb. Due to the close  
184 apposition of  $\beta$ -,  $\alpha$ - and  $\delta$ -cell membranes, we were unable to accurately assign cell-type  
185 specificity to **LUXendin645**. Instead, using cell clusters plated onto coverslips, we could  
186 better discern **LUXendin645** labeling, revealing GLP1R expression in  $18 \pm 6\%$  of  $\alpha$ -cells  
187 (Fig. 4d–f), higher than that shown before using antibodies<sup>19,34</sup> and reporter genes<sup>7</sup>. Notably,  
188 GLP1R-expressing  $\alpha$ -cells tended to adjoin, whereas those without the receptor were next to  
189  $\beta$ -cells. Confirming previous findings, a majority ( $86 \pm 3\%$ ) of  $\beta$ -cells were positive for  
190 **LUXendin645** (Fig 4d-f).<sup>7,19</sup>

191 We wondered whether fixation required for immunostaining might increase background  
192 fluorescence and decrease **LUXendin645** signal such that GLP1R detection sensitivity was  
193 reduced. To circumvent this, studies were repeated in live islets where **LUXendin645** signal  
194 was found to be much brighter and background almost non-existent. GLP1R was detected in  
195  $26.2 \pm 1.1\%$  of non- $\beta$ -cells (Fig 4g, h) using *Ins1Cre<sup>Thor</sup>;R26<sup>mTmG</sup>* reporter mice in which  $\beta$ -  
196 cells are labeled green and all other cell types are labeled red following Cre-mediated  
197 recombination. Once adjusted for the previously reported GLP1R expression in  $\delta$ -cells  
198 (assuming 100%), which constitute  $\sim 5$ -10% of the islet population,<sup>35</sup> this leaves  $\sim 16$ -21% of  
199 GLP1R+  $\alpha$ -cells, reflecting results obtained with immunostaining of dissociated islets. This  
200 was not an artefact of optical section, since two-photon islet reconstructions showed similar  
201 absence of **LUXendin645** staining in discrete regions near the surface (where  $\alpha$ -cells  
202 predominate) (Movie S1).

### 203 **LUXendin645 and Luxendin651 reveal higher-order GLP1R organization**

204 By combining **LUXendin645** with Super-Resolution Radial Fluctuations (SRRF) analysis,<sup>36</sup>  
205 GLP1R could be imaged at super-resolution using streamed images ( $\sim 1000$ ) from a  
206 conventional widefield microscope (Fig. 5a). To image endogenous GLP1R at  $< 100$  nm  
207 lateral resolution, we combined STED nanoscopy with **LUXendin651**, which bears silicon  
208 rhodamine (SiR) instead of Cy5. **LUXendin651** produced bright labeling of wild-type but not  
209 *Glp1r<sup>(GE)-/-</sup>* islets, with an identical distribution to **LUXendin645** (Supplementary Fig. S1).  
210 Incubation of MIN6 cells with **LUXendin651** and subsequent fixation allowed STED imaging  
211 of the endogenous GLP1R with a FWHM =  $70 \pm 10$  nm (Fig. 5b, c). STED snapshots of MIN6  
212  $\beta$ -cells revealed GLP1R distribution with unprecedented detail: receptors were not randomly  
213 arranged but rather tended to organize into nanodomains with neighbors (Fig. 5b, c). This  
214 was confirmed using the F- and G-functions, which showed a non-random and more  
215 clustered GLP1R distribution (Fig. 5d, e). Differences in GLP1R expression level and pattern  
216 could clearly be seen between neighboring cells with a subpopulation possessing highly  
217 concentrated GLP1R clusters (Fig. 5f).

218 Finally, to test whether **LUXendin645** and **LUXendin651** would be capable of tracking  
219 GLP1Rs in live cells, we performed single-molecule microscopy experiments in which  
220 individual receptors labeled with either fluorescent probe were imaged by total internal  
221 reflection fluorescence (TIRF) microscopy.<sup>37,38</sup> Both probes allowed GLP1R to be tracked at  
222 the single-molecule level in CHO-K1-SNAP\_GLP1R cells, but brightness and bleaching  
223 precluded longer recordings with **LUXendin645** (Fig. 5g and Supplementary Movies S2,  
224 S3). By combining single-particle tracking with **LUXendin651**, we were able to show that  
225 most GLP1Rs diffuse rapidly at the membrane (Fig. 5g and Supplementary Movie S4).  
226 However, a mean square displacement (MSD) analysis<sup>37</sup> revealed a high heterogeneity in

227 the diffusion of GLP1Rs on the plasma membrane, ranging from virtually immobile receptors  
228 to some displaying features of directed motion (superdiffusion) (Fig. 5h).

### 229 **Altering fluorophore to produce LUXendin555 confers different ligand behavior**

230 Lastly, we explored whether swapping the far-red Cy5/SiR for a TMR dye would be tolerated  
231 to obtain a spectrally orthogonal probe, termed **LUXendin555**. Labeling was detected in  
232 YFP-AD293-SNAP\_GLP1R (Fig. 6a) but not YFP-AD293 cells (Fig. 6b). However, we  
233 noticed a more punctate **LUXendin555** staining pattern when viewed at high-resolutions  
234 (Fig. 6c). Further experiments with MIN6 cells and islets showed similar internalization of the  
235 GLP1R (Fig. 6d), suggesting that **LUXendin555** acts as an agonist, presumably via  
236 interactions mediated by the ectodomain. This was confirmed using cAMP assays where  
237 **LUXendin555** was found to potently activate GLP1R signaling ( $EC_{50}(\text{cAMP}) = 129.8 \text{ nM}$ ;  
238  $95\% \text{ CI} = 56.9\text{--}296.2$ ) (Fig. 6e). Intriguingly, **LUXendin555** potency could be further  
239 increased using a PAM ( $EC_{50}(\text{cAMP}) = 28.4 \text{ nM}$ ;  $95\% \text{ CI} = 11.3\text{--}71.8$ ) (Fig. 6f), suggesting a  
240 unique binding conformation at the orthosteric site compared to agonists such as  
241 Exendin4(1-39), which cannot be allosterically-modulated.<sup>30</sup> As for the other probes,  
242 **LUXendin555** was unable to label *Glpr*<sup>(GE)-/-</sup> islets (Fig. S2).

### 243 **LUXendins label islets *in vivo***

244 We thought that the high quantum yield of TMR, coupled with good two-photon cross-section  
245 and agonistic behaviour might suit **LUXendin555** well to *in vivo* imaging where maintenance  
246 of normoglycemia under anaesthesia can be an advantage for some experiments. Two-  
247 photon imaging was applied to an anaesthetized mouse to allow visualization of the intact  
248 pancreas, exposed through an abdominal incision (Fig. 6g). Vessels and nuclei were first  
249 labeled using FITC-dextran and Hoechst before injecting **LUXendin555** intravenously.  
250 Labeling occurred rapidly within 5 min post-injection, produced intense membrane staining  
251 confined to the islet where GLP1R is expressed (Fig. 6h), and normoglycemia was  
252 maintained (250 mg/dl). No obvious internalization could be seen, most likely reflecting the  
253 time of exposure to **LUXendin555**, as well as the concentration achieved *in vivo* at the islet.

## 254 DISCUSSION

255 In the present study, we synthesize and validate far-red fluorescent labels, termed  
256 **LUXendins** for the real-time detection of GLP1R in live cells. Nanomolar concentrations of  
257 **LUXendin645** and **LUXendin651** led to intense membrane-labeling of the GLP1R, with best  
258 in class tissue penetration and signal-to-noise ratio, as well as super-resolution capability.  
259 Notably, **LUXendin645** and **LUXendin651** did not activate the GLP1R unless agonist  
260 activity is conferred with the widely-available PAM BETP. **LUXendin645** and **LUXendin651**  
261 are highly specific, as shown using a novel CRISPR-Cas9 mouse line lacking GLP1R  
262 expression. Lastly, the analogous compound **LUXendin555** bearing a different fluorophore  
263 unusually displays agonistic activity, expanding the color palette and activity profile without  
264 changing the peptidic pharmacophore.

265 Compared to present chemical biology approaches, **LUXendins** possess a number of  
266 advantages for GLP1R labeling, which generally rely on Exendin4(1-39) labeled with for  
267 instance Cy3, Cy5 or FITC.<sup>19-21,30</sup> Firstly, the use of an antagonist encourages receptor  
268 recycling back to the membrane and retains receptor at the cell surface, which likely  
269 increases detection capability. Secondly, the GLP1R is not activated, meaning that results  
270 can be interpreted in the absence of potentially confounding cell signaling, such as that  
271 expected with agonists.<sup>19</sup> Thirdly, Cy5 occupies the far-red range, leading to less  
272 background fluorescence, increasing depth penetration due to reduced scatter, and avoiding  
273 the use of more phototoxic wavelengths.<sup>39</sup> Together, these desirable properties open up the  
274 possibility to image expression and trafficking of native GLP1R over extended periods of  
275 time, when **LUXendins** are used in conjunction with a PAM.

276 To test the specificity of **LUXendins**, we used CRISPR-Cas9 genome-editing to globally  
277 knock out the GLP1R in mice. Protein deletion was confirmed by absence of detectable  
278 GLP1R signal following labeling with monoclonal antibody, **LUXendin555**, **LUXendin645**  
279 and **LUXendin651**. While *Glp1r*<sup>-/-</sup> animals already exist and have made important  
280 contributions to our understanding of incretin biology, they were produced using a targeted  
281 mutation to replace exons encoding transmembrane regions 1 and 3 (encoded by exons 5  
282 and 7), presumably leading to deletion of the introns in between (~6.25 kb).<sup>40</sup> By contrast,  
283 *Glp1r*<sup>(GE)-/-</sup> mice possess intact introns. Since introns contain regulatory elements, such as  
284 distant-acting enhancers<sup>41</sup>, miRNAs<sup>42</sup> and lncRNAs,<sup>43</sup> their loss in transgenic knockouts  
285 could have wider influence on the transcriptome. GLP1R knock-out mice might therefore be  
286 useful alongside conventional approaches for validating GLP1R reagents, including  
287 antibodies, agonist and antagonist, and derivatives thereof.

288 Demonstrating the excellent sensitivity of the Cy5-linked **LUXendin645** in particular, we  
289 were able to detect GLP1R in ~20% of  $\alpha$ -cells. Understanding  $\alpha$ -cell GLP1R expression  
290 patterns is important because incretin-mimetics reduce glucagon secretion,<sup>44</sup> which would  
291 otherwise act to aggravate blood glucose levels. However, previous studies using  
292 antibodies, reporter animals and agonist-fluorophores have shown only ~1-10% GLP1R  
293 expression in mouse and rat  $\alpha$ -cells, in line with the low transcript abundance<sup>7,19,33,45</sup>, despite  
294 reports that GLP-1 can directly suppress glucagon release.<sup>34,46</sup> Our data are in general  
295 concordance with these findings, but provide a 2-fold increase in detection capability. This  
296 improvement is likely related to the superior SNR of **LUXendin645**, which increases the  
297 ability to resolve relatively low levels of GLP1R. A recent report showed GLP1R expression  
298 in ~80% of  $\alpha$ -cells using a novel antibody raised against the N-terminal region, with both



299 membrane and cytosolic staining evident<sup>47</sup>. While the reasons for this discrepancy are  
300 unknown, it should be noted that **LUXendin645** binds the orthosteric site and so reports the  
301 proportion of GLP1R that is “signaling competent”<sup>7, 19, 32</sup>.

302 Since **LUXendin645** showed excellent signal-to-noise ratio using conventional  
303 epifluorescence, it was highly amenable to SRRF analysis. As such, **LUXendin645** and its  
304 congeners open up the possibility to image the GLP1R at super-resolution using simple  
305 widefield microscopy available in most laboratories. For stimulated emission depletion  
306 (STED) microscopy experiments, Cy5 was replaced with SiR to give **LUXendin651**. STED  
307 imaging showed that endogenous GLP1R possess a higher structural order, namely  
308 organization into nanodomains at the cell membrane. The presence of nanodomains under  
309 non-stimulated conditions might reflect differences in palmitoylation, which has recently been  
310 shown to influence GLP1R membrane distribution in response to agonists.<sup>48</sup> Notably, a  
311 subpopulation of  $\beta$ -cells appeared to possess highly-concentrated GLP1R clusters. It will be  
312 important in the future to investigate whether this is a cell autonomous heterogenous trait, or  
313 instead reflects biased orientation of membranes toward specific  $\beta$ -cells. Lastly, both  
314 **LUXendin645** and **LUXendin651** allowed GLP1Rs to be imaged in live cells by single-  
315 molecular microscopy, revealing variability in their diffusion at the plasma membrane.  
316 Particle tracking analyses segregated GLP1R into four different populations based upon  
317 diffusion mode, in keeping with data from beta adrenergic receptors.<sup>37</sup> Together, these  
318 experiments provide the first super-resolution characterization of a class B GPCR and  
319 suggest a degree of complexity not readily appreciated with previous approaches.

320 Intriguingly, we saw that swapping Cy5 for a TMR moiety to give **LUXendin555** completely  
321 changed the pharmacological behavior. The reasons for this are unknown, but we speculate  
322 that the rhodamine scaffold engages a secondary binding site in the GLP1R ectodomain,  
323 leading to activation. This finding is remarkable because it suggests that the agonist  $\rightarrow$   
324 antagonist switch that occurs following removal of eight *N*-terminal amino acids (as  
325 physiologically mediated by the protease DPP-4)<sup>49</sup> can be counteracted simply by installing  
326 a *C*-terminal linked rhodamine fluorophore, with implications for the design of more stable  
327 GLP1R activators. More generally, this shift in compound behaviour following a fluorophore  
328 modification serves as another instructive example for the thorough validation of all new  
329 chemical labels.<sup>50</sup> Nonetheless, **LUXendin555** possessed advantageous properties for *in*  
330 *vivo* imaging including maintenance of relatively stable glycemia, good two-photon cross-  
331 section and high quantum yield.

332 In summary, we provide a comprehensively-tested and unique GLP1R detection toolbox  
333 consisting of far-red antagonist labels, **LUXendin645** and **LUXendin651**, an agonist  
334 **LUXendin555**, and knockout *Glp1r*<sup>(GE)-/-</sup> animals. Using these freely-available probes, we  
335 provide an updated view of GLP1R organization, with relevance for the treatment of complex  
336 metabolic diseases such as obesity and diabetes, as well as production of more stable  
337 GLP1R activators. Thus, the stage is set for visualizing GLP1R in various tissues using a  
338 range of imaging techniques, as well as the production of novel peptidic labels and agonists.

339

## 340 METHODS

### 341 Synthesis

342 Solid-phase peptide synthesis of S39C-Exendin4(9-39) was performed as previously  
343 reported.<sup>29</sup> Maleimide-conjugated-6-TMR, -6-SiR and -Cy5 were obtained by TSTU  
344 activation of the corresponding acids and reaction with 1-(2-amino-ethyl)-pyrrole-2,5-dione  
345 (TFA salt, Aldrich). Fluorophore coupling *via* thiol-maleimide chemistry to peptides was  
346 performed in PBS. All compounds were characterized by HRMS and purity was assessed to  
347 be >95% by HPLC. Extinction coefficients were based upon known manufacturer bulk  
348 material measures for TMR-Mal, Cy5-Mal (both Lumiprobe) and SiR-Mal (Spirochrome).  
349 Details for synthesis including further characterization of all **LUXendins** are detailed in the  
350 Supporting Information. **LUXendin555**, **LUXendin651** and **LUXendin645** are freely  
351 available for academic use upon request.

### 352 Cell culture

354 AD293 cells (Agilent) were maintained in Dulbecco's Modified Eagles medium (DMEM)  
355 supplemented with 10% fetal calf serum (FCS), 1% L-glutamine and 1%  
356 penicillin/streptomycin. CHO-K1 cells (a kind gift from Dr Ben Jones, Imperial College  
357 London) stably expressing the human SNAP\_GLP1R (Cisbio) (CHO-K1-SNAP\_GLP1R)  
358 were maintained in DMEM supplemented with 10% FCS, 1% penicillin/streptomycin, 500  
359 µg/mL G418, 5 mM D-glucose, 10 mM HEPES and 1% nonessential amino acids. MIN6 β-  
360 cells (a kind gift from Prof. Jun-ichi Miyazaki, Osaka University) were maintained in DMEM  
361 supplemented with 15% FCS, 25 mM D-glucose, 71 µM BME, 2 mM L-glutamine, 100 U/mL  
362 penicillin, and 100 µg/mL streptomycin. INS1 832/3 CRISPR-deleted for the endogenous  
363 GLP1R locus (a kind gift from Dr. Jacqui Naylor, MedImmune)<sup>51</sup> were transfected with  
364 human SNAP\_GLP1R, before FACS of the SNAP-Surface488-positive population and  
365 selection using G418.<sup>48</sup> The resulting SNAP\_GLP1R\_INS1<sup>GLP1R-/-</sup> cells were maintained in  
366 RPMI-1640 supplemented with 10% FBS, 10 mM HEPES, 2 mM L-glutamine, 1 mM  
367 pyruvate, 72 µM β-mercaptoethanol, 1% penicillin/streptomycin and 500 µg/mL G418.

### 368 Animals

369 *Glp1r*<sup>(GE)-/-</sup>: CRISPR-Cas9 genome-editing was used to introduce a single base pair deletion  
370 into exon 1 of the *Glp1r* locus. Fertilized eggs of female Cas9-overexpressing mice (strain  
371 *Gt(ROSA)26Sor<sup>tm1.1(CAG-cas9\*,-EGFP)Fezh/J</sup>*) were harvested following super-ovulation. Modified  
372 single-guide RNA (Synthego) targeting exon 1 of *Glp1r* and a single-stranded repair-  
373 template were injected at 20 ng/µl into the pronucleus of embryos at the 1-cell stage. In  
374 culture, 80% of embryos reached the 2-cell stage and were transplanted into surrogate mice.  
375 The targeted locus of offspring was analyzed by PCR and sequencing. Besides the insertion  
376 of the repair template, deletions of up to 27 nucleotides could be detected in 2 out of 6  
377 offspring. Design of the repair template will be described elsewhere. Off-target sites were  
378 predicted using the CRISPR Guide Design Tool ([crispr.mit.edu](http://crispr.mit.edu)). Loci of the top ten off-target  
379 hits were amplified by PCR and analyzed *via* Sanger sequencing. Founder animals carrying  
380 alleles with small deletions were backcrossed to wild type animals (strain C57BL/6J) for 1–2  
381 generations to outbreed affected off-targets and then bred to homozygosity. Animals with the  
382 larger deletion of 27 nucleotides were not taken forward, as GLP1R protein was still present.  
383 Animals were born in Mendelian ratios and genotyping was performed using Sanger

384 sequencing. Animals were bred as heterozygous pairs to ensure *Glp1r*<sup>+/+</sup> littermates.  
385 *Glp1r*<sup>(GE)-/-</sup> animals are freely available for academic use, subject to a Material Transfer  
386 Agreement.

387 *Ins1Cre*<sup>Thor</sup>;R26<sup>mT/mG</sup>: To allow identification of  $\beta$ - and non- $\beta$ -cells, *Ins1Cre*<sup>Thor</sup> animals with  
388 Cre knocked-in at the *Ins1* locus (strain B6(Cg)-*Ins1*<sup>tm1.1(cre)Thor/J</sup>) were crossed with R26<sup>mT/mG</sup>  
389 reporter mice (strain B6.129(Cg)-*Gt(ROSA)26Sor*<sup>tm4(ACTB-tdTomato,-EGFP)Lo0/J</sup>). Cre-dependent  
390 excision of the floxed allele results in deletion of tdTomato, expression of membrane-  
391 localized GFP and thus identification of recombined and non-recombined cells.

392 All studies were performed with 6-12 week old male and female animals, and regulated by  
393 the Animals (Scientific Procedures) Act 1986 of the U.K. Approval was granted by the  
394 University of Birmingham's Animal Welfare and Ethical Review Body.

### 395 **Islet isolation**

396 Islets were isolated from male and female *Glp1r*<sup>(GE)-/-</sup> and *Ins1Cre*<sup>Thor</sup>;R26<sup>mT/mG</sup> mice, as well  
397 as CD1 wild-type animals, maintained under specific-pathogen free conditions, with *ad lib*  
398 access to food and water. Briefly, animals were humanely euthanized before injection of  
399 collagenase 1 mg/mL (Serva NB8) into the bile duct. Following removal of the inflated  
400 pancreas and digestion for 12 min at 37 °C, islets were separated using a Histopaque  
401 (Sigma-Aldrich) gradient. Islets were cultured in RPMI medium containing 10% FCS, 100  
402 units/mL penicillin, and 100  $\mu$ g/mL streptomycin.

### 403 **Binding and potency assays**

404 Binding assays were performed in transiently-transfected YFP-AD293-SNAP\_GLP1R cells  
405 (using PolyJet reagent; SignaGen). Increasing concentrations of compound were applied for  
406 60 min, before imaging using a Zeiss LSM880 meta-confocal microscope configured with  
407 GaAsP detectors and 10 $\times$ /0.45 W, 40 $\times$ /1.00 W and 63 $\times$ /1.20 W objectives. YFP, TMR  
408 (**LUXendin555**) and Cy5 (**LUXendin645**) were excited using  $\lambda$  = 514 nm,  $\lambda$  = 561 nm and  $\lambda$   
409 = 633 nm lasers, respectively. Emitted signals were captured at  $\lambda$  = 519–574 nm,  $\lambda$  = 570–  
410 641 nm and  $\lambda$  = 638–759 nm for YFP, TMR (**LUXendin555**) and Cy5 (**LUXendin645**),  
411 respectively. Control experiments were performed in YFP-AD293-SNAP cells, as above.

412 Potency for cAMP generation and inhibition was tested in heterologous expression systems,  
413 comprising either stable CHO-K1-SNAP\_GLP1R cells or transiently-transfected YFP-  
414 AD293-SNAP\_GLP1R cells, as previously described.<sup>29</sup> Briefly, cells were incubated with  
415 increasing concentrations of compound +/- allosteric modulator for 30 min, before  
416 harvesting, lysis and measurement of cAMP using cAMP-Glo<sup>TM</sup> Assay (Promega), according  
417 to the manufacturer's instructions. *EC*<sub>50</sub> values were calculated using log concentration-  
418 response curves fitted with a three-parameter equation.

### 419 **Live imaging**

420 Islets were incubated for 1 h at 37 °C in culture medium supplemented with either 100-250  
421 nM **LUXendin555**, 50-100 nM **LUXendin645** or 100 nM **LUXendin651**, based upon binding  
422 assays. Islets were imaged using either a Zeiss LSM780 or LSM880 microscope, as above  
423 (**LUXendin651** was imaged as for **LUXendin645**). *Ins1Cre*<sup>Thor</sup>;R26<sup>mT/mG</sup> islets were excited  
424 at  $\lambda$  = 488 nm (emission,  $\lambda$  = 493-555 nm) and  $\lambda$  = 561 nm (emission,  $\lambda$  = 570-624 nm) for

425 mGFP and tdTomato, respectively. Two-photon imaging of **LUXendin645** was performed  
426 using a Zeiss LSM 880 NLO equipped with a Spectra-Physics Insight X3 femtosecond-  
427 pulsed laser and 20x/1.00 W objective. Excitation was performed at  $\lambda = 800$  nm and emitted  
428 signals detected at  $\lambda = 638$ -759 nm.

### 429 **cAMP imaging**

430 Islets were transduced with adenovirus harboring the FRET sensor, Epac2-camps, before  
431 imaging using a Crest X-Light spinning disk system coupled to a Nikon Ti-E base and  
432 10x/0.4 NA objective. Excitation was delivered at  $\lambda = 430$ –450 nm using a Lumencor Spectra  
433 X light engine. Emitted signals were detected at  $\lambda = 460$ –500 and  $\lambda = 520$ –550 nm for  
434 Cerulean and Citrine, respectively, using a Photometrics Delta Evolve EM-CCD. Imaging  
435 was performed in HEPES-bicarbonate buffer, containing (in mmol/L) 120 NaCl, 4.8 KCl, 24  
436 NaHCO<sub>3</sub>, 0.5 Na<sub>2</sub>HPO<sub>4</sub>, 5 HEPES, 2.5 CaCl<sub>2</sub>, 1.2 MgCl<sub>2</sub>, and 3–17 D-glucose. Vehicle  
437 (H<sub>2</sub>O), Exendin4(1-39) (10-20 nM) or Liraglutide (10 nM) were applied at the indicated time  
438 points, with forskolin (10  $\mu$ M) acting as a positive control.

### 439 **Immunostaining**

440 **LUXendin555**- or **LUXendin645**-treated cells or tissue were fixed for 60 min in 4%  
441 paraformaldehyde. Primary antibodies were applied overnight at 4 °C in PBS + 0.1% Triton  
442 + 1% BSA. Secondary antibodies were applied in the same buffer for 1 h at room  
443 temperature, before mounting on slides using Vectashield Hardset containing DAPI. Primary  
444 antibodies were mouse monoclonal anti-GLP1R 1:30 (Iowa DHSB; mAb #7F38), rabbit anti-  
445 insulin 1:500 (Cell Signaling Technology, #3014), mouse monoclonal anti-glucagon 1:2000  
446 (Sigma-Aldrich, #G2654) and mouse anti-somatostatin 1:5000 (Invitrogen, #14-9751-80).  
447 Secondary antibodies were goat anti-mouse Alexa Fluor 568 and donkey anti-rabbit DyLight  
448 488 1:1000. Images were captured using an LSM880 meta-confocal microscope. Alexa  
449 Fluor 488 and Alexa Fluor 568 were excited at  $\lambda = 488$  nm and  $\lambda = 568$  nm, respectively.  
450 Emitted signals were detected at  $\lambda = 500$ –550 nm (Alexa Fluor 488) and  $\lambda = 519$ –574 nm  
451 (Alexa Fluor 568).

### 452 **Super-resolution microscopy**

453 *SRRF*: MIN6 were treated with **LUXendin645** before fixation and mounting on slides using  
454 Vectashield Hardset containing DAPI. Imaging was performed using a Crest X-Light  
455 spinning disk system in bypass (widefield) mode. Excitation was delivered at  $\lambda = 640/30$  nm  
456 through a 63x/1.4 NA objective using a Lumencor Spectra X light engine. Emission was  
457 collected at  $\lambda = 700/75$  nm using a Photometrics Delta Evolve EM-CDD. A 1000 image  
458 sequence was captured (~ 2 min) before offline super resolution radial fluctuation (SRRF)  
459 analysis to generate a single super-resolution snapshot using the NanoJ plugin for ImageJ  
460 (NIH).<sup>36</sup>

461 *Stimulated emission depletion (STED) microscopy*: MIN6 cells were treated with 100, 200  
462 and 400 nM **LUXendin651** before fixation (4% paraformaldehyde, 20 min). Cells were  
463 mounted in Mowiol supplemented with DABCO and imaged on an Abberior STED  
464 775/595/RESOLFT QUAD scanning microscope (Abberior Instruments GmbH, Germany)  
465 equipped with STED lines at  $\lambda = 595$  and  $\lambda = 775$  nm, excitation lines at  $\lambda = 355$  nm, 405 nm,  
466 485 nm, 561 nm, and 640 nm, spectral detection, and a UPlanSApo 100x/1.4 oil immersion  
467 objective lens. Following excitation at  $\lambda = 640$  nm, fluorescence was acquired in the spectral

468 window  $\lambda = 650\text{-}800$  nm. Deconvolution was performed with Richardson-Lucy algorithm on  
469 Inspector software. FWHM was measured on raw data and calculated using OriginPro 2017  
470 software with Gaussian fitting (n=15 profiles). Spatial GLP1R expression patterns were  
471 analyzed using the F- and G-functions, where F = distance between an object of interest and  
472 its nearest neighbor, and G = distance from a given position to the nearest object of interest  
473 (FIJI Spatial Statistic 2D/3D plugin).<sup>52</sup> Both measures were compared to a random  
474 distribution of the same measured objects, with a shift away from the mean +/- 95%  
475 confidence intervals indicating a non-random or clustered organization (*i.e.* more space or  
476 smaller distance between objects).

477 *Single-molecule microscopy:* For single-molecule experiments, CHO-K1-SNAP\_GLP1R cells  
478 were seeded onto 25 mm clean glass coverslips at a density of  $3 \times 10^5$  per well. On the  
479 following day, cells were labeled in culture medium with 100 pM **LUXendin645** or  
480 **LUXendin651** for 20 min. At the end of the incubation, cells were washed 3x 5 min in culture  
481 medium. Cells were then imaged at 37 °C in phenol-red free Hank's balanced salt solution,  
482 using a custom built total internal reflection fluorescence microscope (Cairn Research)  
483 based on an Eclipse Ti2 (Nikon, Japan) equipped with an EMCCD camera (iXon Ultra,  
484 Andor), 637 nm diode laser, and a 100x oil-immersion objective (NA 1.49, Nikon). Image  
485 sequences were acquired with an exposure time of 60 ms. Single-molecule image  
486 sequences were analyzed with an automated particle detection software (utrack) in the  
487 MATLAB environment, as previously described.<sup>53,54</sup> Data were further analyzed using  
488 custom MATLAB algorithms, as previously described.<sup>37,55</sup>

## 489 **Two-photon *in vivo* imaging**

490 A 7 week old female C57BL/6J mouse was anesthetized with isoflurane and a small, 1 cm  
491 vertical incision was made at the level of the pancreas. The exposed organ was orientated  
492 underneath the animal and pressed against a 50 mm glass-bottom dish for imaging on an  
493 inverted microscope. Body temperature was maintained using heat pads and heating  
494 elements on the objective. The mouse received Hoechst 33342 (1 mg/kg in PBS) to label  
495 nuclei, a 150 kDalton fluorescein-conjugated dextran (1 mg/kg in PBS) to label vasculature,  
496 and 75  $\mu\text{L}$  of 30  $\mu\text{M}$  **LUXendin555** via retro-orbital IV injection. Images were collected using  
497 a Leica SP8 microscope, equipped with a 25x/0.95 NA objective and Spectra Physics  
498 MaiTai DeepSee multiphoton laser. Excitation was delivered at  $\lambda = 850$  nm, with signals  
499 collected with a HyD detector at  $\lambda = 460/50$ ,  $\lambda = 525/50$ ,  $\lambda = 624/40$  nm for Hoechst, FITC  
500 and **LUXendin555**, respectively. All *in vivo* imaging experiments were performed with  
501 approval and oversight from the Indiana University Institutional Animal Care and Use  
502 Committee (IACUC).

## 503 **Statistical analyses**

504 Measurements were performed on discrete samples unless otherwise stated. All analyses  
505 were conducted using GraphPad Prism software. Unpaired or paired Students t-test was  
506 used for pairwise comparisons. Multiple interactions were determined using one-way  
507 ANOVA followed by Dunn's or Sidak's posthoc tests (accounting for degrees of freedom).

508 **Data availability**

509 The datasets generated during and/or analysed during the current study are available from  
510 the corresponding author on reasonable request.

511

512 REFERENCES

- 513 1. Baggio, L.L. & Drucker, D.J. Biology of incretins: GLP-1 and GIP. *Gastroenterology*  
514 **132**, 2131-57 (2007).
- 515 2. Campbell, J.E. & Drucker, D.J. Pharmacology, physiology, and mechanisms of  
516 incretin hormone action. *Cell Metab* **17**, 819-837 (2013).
- 517 3. Parker, H.E. et al. Molecular mechanisms underlying bile acid-stimulated glucagon-  
518 like peptide-1 secretion. *British Journal of Pharmacology* **165**, 414-23 (2012).
- 519 4. Leech, C.A. et al. Molecular physiology of glucagon-like peptide-1 insulin  
520 secretagogue action in pancreatic beta cells. *Progress in Biophysics and Molecular*  
521 *Biology* **107**, 236-47 (2011).
- 522 5. MacDonald, P.E. et al. The multiple actions of GLP-1 on the process of glucose-  
523 stimulated insulin secretion. *Diabetes* **51 Suppl 3**, S434-42 (2002).
- 524 6. Cork, S.C. et al. Distribution and characterisation of Glucagon-like peptide-1 receptor  
525 expressing cells in the mouse brain. *Mol Metab* **4**, 718-31 (2015).
- 526 7. Richards, P. et al. Identification and Characterization of GLP-1 Receptor-Expressing  
527 Cells Using a New Transgenic Mouse Model. *Diabetes* **63**, 1224-1233 (2013).
- 528 8. Giepmans, B.N., Adams, S.R., Ellisman, M.H. & Tsien, R.Y. The fluorescent toolbox  
529 for assessing protein location and function. *Science* **312**, 217-24 (2006).
- 530 9. Yang, G. et al. Genetic targeting of chemical indicators in vivo. *Nat Methods* **12**, 137-  
531 139 (2015).
- 532 10. Lukinavičius, G. et al. A near-infrared fluorophore for live-cell super-resolution  
533 microscopy of cellular proteins. *Nature Chemistry* **5**, 132-139 (2013).
- 534 11. Los, G.V. et al. HaloTag: A Novel Protein Labeling Technology for Cell Imaging and  
535 Protein Analysis. *ACS Chemical Biology* **3**, 373-382 (2008).
- 536 12. Lang, K. et al. Genetic Encoding of Bicyclononynes and trans-Cyclooctenes for Site-  
537 Specific Protein Labeling in Vitro and in Live Mammalian Cells via Rapid Fluorogenic  
538 Diels–Alder Reactions. *Journal of the American Chemical Society* **134**, 10317-10320  
539 (2012).
- 540 13. Jewett, J.C. & Bertozzi, C.R. Cu-free click cycloaddition reactions in chemical  
541 biology. *Chem Soc Rev* **39**, 1272-9 (2010).
- 542 14. Lukinavicius, G. et al. Fluorogenic Probes for Multicolor Imaging in Living Cells. *J Am*  
543 *Chem Soc* **138**, 9365-8 (2016).
- 544 15. Lukinavicius, G. et al. Fluorogenic probes for live-cell imaging of the cytoskeleton.  
545 *Nat Methods* **11**, 731-3 (2014).
- 546 16. Karch, S. et al. A New Fluorogenic Small-Molecule Labeling Tool for Surface  
547 Diffusion Analysis and Advanced Fluorescence Imaging of  $\beta$ -Site Amyloid Precursor  
548 Protein-Cleaving Enzyme 1 Based on Silicone Rhodamine: SiR-BACE1. *Journal of*  
549 *Medicinal Chemistry* **61**, 6121-6139 (2018).
- 550 17. Pyke, C. et al. GLP-1 receptor localization in monkey and human tissue: novel  
551 distribution revealed with extensively validated monoclonal antibody. *Endocrinology*  
552 **155**, 1280-90 (2014).
- 553 18. Pyke, C. & Knudsen, L.B. The glucagon-like peptide-1 receptor--or not?  
554 *Endocrinology* **154**, 4-8 (2013).
- 555 19. Lehtonen, J., Schäffer, L., Rasch, M.G., Hecksher-Sørensen, J. & Ahnfelt-Rønne, J.  
556 Beta cell specific probing with fluorescent exendin-4 is progressively reduced in type  
557 2 diabetic mouse models. *Islets* **7**, e1137415 (2016).
- 558 20. Clardy, S.M. et al. Fluorescent Exendin-4 Derivatives for Pancreatic  $\beta$ -Cell Analysis.  
559 *Bioconjugate Chemistry* **25**, 171-177 (2013).
- 560 21. Clardy, S.M. et al. Rapid, high efficiency isolation of pancreatic ss-cells. *Sci Rep* **5**,  
561 13681 (2015).
- 562 22. Kleiner, S. et al. Mice harboring the humanSLC30A8R138X loss-of-function mutation  
563 have increased insulin secretory capacity. *Proceedings of the National Academy of*  
564 *Sciences* **115**, E7642-E7649 (2018).

- 565 23. Kim, J. et al. Amino Acid Transporter Slc38a5 Controls Glucagon Receptor Inhibition-  
566 Induced Pancreatic  $\alpha$  Cell Hyperplasia in Mice. *Cell Metabolism* **25**, 1348-1361.e8  
567 (2017).
- 568 24. Aroor, A. & Nistala, R. Tissue-Specific Expression of GLP1R in Mice: Is the Problem  
569 of Antibody Nonspecificity Solved? *Diabetes* **63**, 1182-1184 (2014).
- 570 25. Drucker, Daniel J. The Cardiovascular Biology of Glucagon-like Peptide-1. *Cell*  
571 *Metabolism* **24**, 15-30 (2016).
- 572 26. Armstrong, M.J. et al. Liraglutide safety and efficacy in patients with non-alcoholic  
573 steatohepatitis (LEAN): a multicentre, double-blind, randomised, placebo-controlled  
574 phase 2 study. *The Lancet* **387**, 679-690 (2016).
- 575 27. Baggio, L.L. & Drucker, D.J. Glucagon-like peptide-1 receptors in the brain:  
576 controlling food intake and body weight. *Journal of Clinical Investigation* **124**, 4223-  
577 4226 (2014).
- 578 28. Mukai, E. et al. GLP-1 receptor antagonist as a potential probe for pancreatic beta-  
579 cell imaging. *Biochem Biophys Res Commun* **389**, 523-6 (2009).
- 580 29. Podewin, T. et al. Conditional and Reversible Activation of Class A and B G Protein-  
581 Coupled Receptors Using Tethered Pharmacology. *ACS Central Science* **4**, 166-179  
582 (2018).
- 583 30. Jones, B.J. et al. Potent Prearranged Positive Allosteric Modulators of the Glucagon-  
584 like Peptide-1 Receptor. *ChemistryOpen*, 501-505 (2017).
- 585 31. López de Maturana, R., Willshaw, A., Kuntzsch, A., Rudolph, R. & Donnelly, D. The  
586 Isolated N-terminal Domain of the Glucagon-like Peptide-1 (GLP-1) Receptor Binds  
587 Exendin Peptides with Much Higher Affinity than GLP-1. *Journal of Biological*  
588 *Chemistry* **278**, 10195-10200 (2003).
- 589 32. Ban, K. et al. Glucagon-Like Peptide (GLP)-1(9-36)Amide-Mediated Cytoprotection Is  
590 Blocked by Exendin(9-39) Yet Does Not Require the Known GLP-1 Receptor.  
591 *Endocrinology* **151**, 1520-1531 (2010).
- 592 33. DiGruccio, M.R. et al. Comprehensive alpha, beta and delta cell transcriptomes  
593 reveal that ghrelin selectively activates delta cells and promotes somatostatin release  
594 from pancreatic islets. *Molecular Metabolism* **5**, 449-458 (2016).
- 595 34. De Marinis, Y.Z. et al. GLP-1 Inhibits and Adrenaline Stimulates Glucagon Release  
596 by Differential Modulation of N- and L-Type Ca<sup>2+</sup> Channel-Dependent Exocytosis.  
597 *Cell Metabolism* **11**, 543-553 (2010).
- 598 35. Cabrera, O. et al. The unique cytoarchitecture of human pancreatic islets has  
599 implications for islet cell function. *Proceedings of the National Academy of Sciences*  
600 *of the United States of America* **103**, 2334-9 (2006).
- 601 36. Gustafsson, N. et al. Fast live-cell conventional fluorophore nanoscopy with ImageJ  
602 through super-resolution radial fluctuations. *Nat Commun* **7**, 12471 (2016).
- 603 37. Sungkaworn, T. et al. Single-molecule imaging reveals receptor-G protein  
604 interactions at cell surface hot spots. *Nature* **550**, 543-547 (2017).
- 605 38. Calebiro, D. et al. Single-molecule analysis of fluorescently labeled G-protein-  
606 coupled receptors reveals complexes with distinct dynamics and organization. *Proc*  
607 *Natl Acad Sci U S A* **110**, 743-8 (2013).
- 608 39. Pansare, V., Hejazi, S., Faenza, W. & Prud'homme, R.K. Review of Long-  
609 Wavelength Optical and NIR Imaging Materials: Contrast Agents, Fluorophores and  
610 Multifunctional Nano Carriers. *Chem Mater* **24**, 812-827 (2012).
- 611 40. Scrocchi, L.A. et al. Glucose intolerance but normal satiety in mice with a null  
612 mutation in the glucagon-like peptide 1 receptor gene. *Nat Med* **2**, 1254-8 (1996).
- 613 41. Visel, A., Rubin, E.M. & Pennacchio, L.A. Genomic views of distant-acting  
614 enhancers. *Nature* **461**, 199-205 (2009).
- 615 42. Filios, S.R. & Shalev, A.  $\beta$ -Cell MicroRNAs: Small but Powerful. *Diabetes* **64**, 3631-  
616 3644 (2015).
- 617 43. Akerman, I. et al. Human Pancreatic beta Cell lncRNAs Control Cell-Specific  
618 Regulatory Networks. *Cell Metab* **25**, 400-411 (2017).



- 619 44. Nauck, M.A. et al. Normalization of fasting hyperglycaemia by exogenous glucagon-  
620 like peptide 1 (7-36 amide) in type 2 (non-insulin-dependent) diabetic patients.  
621 *Diabetologia* **36**, 741-4 (1993).
- 622 45. Tornehave, D., Kristensen, P., Romer, J., Knudsen, L.B. & Heller, R.S. Expression of  
623 the GLP-1 receptor in mouse, rat, and human pancreas. *J Histochem Cytochem* **56**,  
624 841-51 (2008).
- 625 46. Ramracheya, R. et al. GLP-1 suppresses glucagon secretion in human pancreatic  
626 alpha-cells by inhibition of P/Q-type Ca<sup>2+</sup>  
627 channels. *Physiological Reports* **6**, e13852 (2018).
- 628 47. Zhang, Y. et al. GLP-1 Receptor in Pancreatic alpha Cells Regulates Glucagon  
629 Secretion in a Glucose-Dependent Bidirectional Manner. *Diabetes* (2018).
- 630 48. Buenaventura, T. et al. Agonist binding affinity determines palmitoylation of the  
631 glucagon-like peptide 1 receptor and its functional interaction with plasma membrane  
632 nanodomains in pancreatic beta cells. (2018).
- 633 49. Omar, B. & Ahren, B. Pleiotropic Mechanisms for the Glucose-Lowering Action of  
634 DPP-4 Inhibitors. *Diabetes* **63**, 2196-2202 (2014).
- 635 50. Smith, N.A. et al. Fluorescent Ca<sup>2+</sup>-indicators directly inhibit the Na,K-ATPase and  
636 disrupt cellular functions. *Science Signaling* **11**, eaal2039 (2018).
- 637 51. Naylor, J. et al. Use of CRISPR/Cas9-engineered INS-1 pancreatic beta cells to  
638 define the pharmacology of dual GIPR/GLP-1R agonists. *Biochem J* **473**, 2881-91  
639 (2016).
- 640 52. Zimmer, C. et al. Statistical Analysis of 3D Images Detects Regular Spatial  
641 Distributions of Centromeres and Chromocenters in Animal and Plant Nuclei. *PLoS*  
642 *Computational Biology* **6**, e1000853 (2010).
- 643 53. Jaqaman, K. et al. Robust single-particle tracking in live-cell time-lapse sequences.  
644 *Nature Methods* **5**, 695-702 (2008).
- 645 54. Sungkaworn, T., Rieken, F., Lohse, M.J. & Calebiro, D. High-resolution  
646 Spatiotemporal Analysis of Receptor Dynamics by Single-molecule Fluorescence  
647 Microscopy. *Journal of Visualized Experiments* (2014).
- 648 55. Treppiedi, D. et al. Single-Molecule Microscopy Reveals Dynamic FLNA Interactions  
649 Governing SSTR2 Clustering and Internalization. *Endocrinology* **159**, 2953-2965  
650 (2018).
- 651 56. Zhang, Y. et al. Cryo-EM structure of the activated GLP-1 receptor in complex with a  
652 G protein. *Nature* **546**, 248-253 (2017).
- 653

654 **ACKNOWLEDGMENTS**

655 We thank Bettina Mathes and Alexandra Teslenko for excellent synthetic support. D.J.H.  
656 was supported by a Diabetes UK R.D. Lawrence (12/0004431) Fellowship, a Wellcome  
657 Trust Institutional Support Award, MRC Confidence in Concept, MRC (MR/N00275X/1)  
658 Project and Diabetes UK (17/0005681) Project Grants. ST was supported by an MRC  
659 Project Grant (MR/N02589X/1). B.H. was supported by the Wellcome Trust (095101,  
660 200837 and 106130). A.K.L. was supported by R03 DK115990 (to A.K.L.) and Human Islet  
661 Research Network UC4 DK104162 (to A.K.L.; RRID:SCR\_014393). Intravital microscopy  
662 core services were supported by NIH NIDDK Grant P30 DK097512 to the Indiana University  
663 School of Medicine. A.T. and B.J. were funded by an MRC Project Grant (MR/R010676/1).  
664 D.C. was funded by the Deutsche Forschungsgemeinschaft (SFB/Transregio 166–Project  
665 C1) and a Wellcome Trust Senior Research Fellowship. This project has received funding  
666 from the European Research Council (ERC) under the European Union’s Horizon 2020  
667 research and innovation programme (Starting Grant 715884 to D.J.H.). We thank Prof Anna  
668 Gloyn (University of Oxford) for provision of reagents, Dr Birgit Koch (MPI, Heidelberg) for  
669 helpful discussions on *Glp1r*<sup>(GE)-/-</sup> mice and Dr Jacqueline Naylor (MedImmune) for  
670 generation of parental SNAP\_GLP1R-INS1<sup>GLP1R-/-</sup> cells.

671 **CONTRIBUTIONS**

672 J.A., K.J., T.P., J.B. and D.J.H. devised the studies. J.A., A.A., D.N., N.H.F.F., F.B.A., S.T.,  
673 Z.S., B.H., A.T., T.P., J.B. and D.J.H. performed experiments and analyzed data. J.A. and  
674 A.B. generated novel mice. B.J.J. provided reagents. Z.K. and E.D’E. performed super-  
675 resolution imaging. C.A.R. and A.K.L. performed *in vivo* imaging experiments. D.C.  
676 supervised and analyzed single-molecule microscopy experiments. J.A., K.J., T.P., J.B. and  
677 D.J.H. supervised the work. J.A., T.P., J.B. and D.J.H. wrote the manuscript with input from  
678 all the authors.

679 **COMPETING INTERESTS**

680 The authors declare no conflict of interest.

681

## 682 FIGURE LEGENDS

683 **Figure 1: Sequence and structure of LUXendin555, LUXendin651 and LUXendin645**  
684 **bound to GLP1R.** LUXendins are based on the antagonist Exendin4(9-39), shown in  
685 complex with GLP1R. The label can be any dye, such as TMR (top), SiR (middle) or Cy5  
686 (bottom) to give **LUXendin555, LUXendin651 and LUXendin645**, respectively. The model  
687 was obtained by using the cryo-EM structure of the activated form of GLP1R in complex with  
688 a G protein (pdb: 5VAI)<sup>56</sup>, with the G protein and the 8 N-terminal amino acids of the ligand  
689 removed from the structure while mutating S39C and adding the respective linker. Models  
690 were obtained as representative cartoons by the in-built building capability of PyMOL (Palo  
691 Alto, CA, USA) without energy optimization. Succinimide stereochemistry is unknown and  
692 neglected for clarity.

693

694 **Figure 2: LUXendin645 binding, signaling and labeling.** **a**, Exendin4(9-39), its S39C  
695 mutant and **LUXendin645** display similar antagonistic properties (n = 3 replicates). **b**,  
696 **LUXendin645** does not activate the GLP1R in CHO-K1-SNAP\_GLP1R cells unless the  
697 positive allosteric modulator (PAM) BETP is present (Exendin4; +ve control) (n = 3 assays).  
698 **c**, **LUXendin645** labels CHO-K1-SNAP\_GLP1R cells with a maximal labeling achieved at  
699 100 nM. **d**, **LUXendin645** signal can be detected in YFP-AD293-SNAP\_GLP1R but not  
700 YFP-AD293 cells (scale bar = 212.5  $\mu$ m) (n = 3 assays). **e**, Representative confocal z-stack  
701 (1  $\mu$ m steps) showing penetration of **LUXendin645** deep into a live pancreatic islet (x-y, x-z  
702 and y-z projections are shown) (n = 4 islets) (scale bar = 37.5  $\mu$ m). **f**, As for (**e**), but two-  
703 photon z-stack (1  $\mu$ m steps) showing the entire volume of an islet labeled with **LUXendin645**  
704 (scale bar = 37.5  $\mu$ m) (n = 9 islets). **g** and **h**, GLP1R is internalized in MIN6 cells when  
705 agonist activity is conferred on **LUXendin645** using the positive allosteric modulator BETP  
706 (scale bar = 21  $\mu$ m) (n = 5 images, 693-722 cells; Student's unpaired t-test) (Bar graph  
707 shows mean  $\pm$  SEM). **i** and **j**, **LUXendin645** signal can be detected even following fixation  
708 and co-localizes with a specific monoclonal antibody against the GLP1R in both islets (n =  
709 13 islets) and MIN6  $\beta$ -cells (n = 6 images, 543 cells) (scale bar = 26  $\mu$ m). **k**, The superior  
710 signal-to-noise-ratio of **LUXendin645** allows more membrane detail to be visualized  
711 compared to antibody (scale bar = 12.5  $\mu$ m). Representative images are shown, with a blue  
712 bar indicating the location of intensity-over-distance measures (the islet was co-stained with  
713 **LUXendin645** + antibody to allow direct comparison) (n = 13 islets). **l** and **m**, **LUXendin645**  
714 co-localizes with the SNAP label, Surface 488, in SNAP\_hGLP1R-INS1<sup>GLP1<sup>-/-</sup></sup>, which are  
715 deleted for the endogenous *Glp1r* (**l**). Pre-treatment with Exendin4(9-39) to internalize the  
716 GLP1R reduces **LUXendin645**-labeling (**m**) (a wash-step was used prior to application of  
717 the label) (scale bar = 10  $\mu$ m) (n = 4-5 images; 57-64 cells). Mean  $\pm$  SE are shown.  
718 \*\*P<0.01.

719

720 **Figure 3: LUXendin645 is highly specific for the GLP1R.** **a**, Schematic showing sgRNA  
721 targeting strategy for the production of *Glp1r*<sup>(GE)<sup>-/-</sup></sup> mice. The sgRNA used targeted *Glp1r* and  
722 the double-strand break mediated by Cas9 lies within exon1 (capital letters); intron shown in  
723 gray. **b**, *Glp1r*<sup>(GE)<sup>-/-</sup></sup> animals harbor a single-nucleotide deletion, as shown by sequencing  
724 traces. **c**, Body weights were similar in male 8 weeks old *Glp1r*<sup>+/+</sup>, *Glp1r*<sup>(GE)<sup>+/-</sup></sup> and *Glp1r*<sup>(GE)<sup>-/-</sup></sup>  
725 littermates (n = 4–8 animals; one-way ANOVA with Bonferroni's post hoc test; F = 0.7982,  
726 DF = 2) (Bar graph shows mean  $\pm$  SEM) **d**, The incretin-mimetic Exendin4(1-39) (10 nM) is

727 unable to significantly potentiate glucose-stimulated insulin secretion in *Glp1r*<sup>(GE)-/-</sup> islets (n =  
728 6 replicates; two-way ANOVA with Sidak's post hoc test; F = 14.96, DF = 2 for *Glp1r*<sup>+/+</sup>, F =  
729 2.968, DF = 2 for *Glp1r*<sup>(GE)-/-</sup>) (Bar graph shows mean ± SEM) **e**, Liraglutide (Lira) does not  
730 stimulate cAMP beyond vehicle (Veh) control in *Glp1r*<sup>(GE)-/-</sup> islets, measured using the FRET  
731 probe Epac2-camps (traces represent mean ± SEM) (n = 14–17 islets). **f**, cAMP area-under-  
732 the-curve (AUC) quantification showing absence of significant Liraglutide-stimulation in  
733 *Glp1r*<sup>(GE)-/-</sup> islets (n = 14–17 islets; Kruskal-Wallis test with Dunn's post hoc test; Kruskal-  
734 Wallis statistic = 7.6, DF = 2) (Box and Whiskers plot shows min-max and median)  
735 (representative images displayed above each bar). **g**, **LUXendin645** and GLP1R antibody  
736 labeling is not detectable in *Glp1r*<sup>(GE)-/-</sup> islets (scale bar = 40 μm) (n = 12–14 islets for each  
737 genotype). \*P<0.05, \*\*P<0.01 and NS, non-significant.

738

739 **Figure 4: LUXendin645 reveals GLP1R expression in a subpopulation of α-cells. a-c,**  
740 **LUXendin645** labeling is widespread throughout the intact islet, co-localizing predominantly  
741 with β-cells (**a**) and α-cells (**b**), but less so with δ-cells (**c**) stained for insulin, glucagon and  
742 somatostatin, respectively (n = 7–9 islets) (scale bar = 26 μm). **d**, Following dissociation of  
743 islets into cell clusters, **LUXendin645** labeling can be more accurately quantified (arrows  
744 highlight cells selected for zoom-in) (scale bar = 26 μm). **e**, Zoom-in of (**d**) showing a  
745 **LUXendin645**- (left) and **LUXendin645**+ (right) α-cell (arrows highlight non-labeled cell  
746 membrane, which is not bounded by a β-cell) (scale bar = 26 μm). **f**, Box-and-whiskers plot  
747 showing proportion of β-cells (INS) and α-cells (GLU) co-localized with **LUXendin645** (n =  
748 5–6 images, 12 cell clusters) (Max-min shown together with the median). **g**,  
749 *Ins1Cre*<sup>Thor</sup>; *R26*<sup>mT/mG</sup> dual fluorophore reporter islets express tdTomato until Cre-mediated  
750 replacement with mGFP, allowing identification of β-cells (~80% of the islet population) and  
751 non-β-cells for live imaging (scale bar = 26 μm). **LUXendin645** highlights GLP1R expression  
752 in nearly all β-cells but relatively few non-β-cells (n = 24 islets, 809 cells). **h**, As for (**g**), but a  
753 zoom-in showing GLP1R expression in some non-β-cells (left) together with quantification  
754 (right) (arrows show **LUXendin645**-labeled non-β cells) (scale bar = 5 μm) (Box and  
755 Whiskers plot shows min-max and median).

756

757 **Figure 5: LUXendin651 and LUXendin645 allow nanoscopic detection of GLP1R**  
758 **distribution and dynamics. a, LUXendin645** allows super-resolution snapshots of MIN6 β-  
759 cells using widefield microscopy combined with Super-Resolution Radial Fluctuations  
760 (SRRF) (n = 3 images) (scale bar = 10 μm). **b** and **c**, Confocal and STED snapshots of  
761 endogenous GLP1R in **LUXendin651**-treated MIN6 cells at ~ 50 nm axial resolution. Note  
762 the presence of punctate GLP1R expression as well as aggregation/clustering in images  
763 captured above (**b**) and close to the coverslip (**c**) using STED microscopy (n = 3 images, 15  
764 cells) (scale bar = 2 μm). **d** and **e**, Spatial analysis of GLP1R expression patterns using the  
765 F-function (**d**) and G-function (**e**) show a non-random distribution (red line) versus a random  
766 model (black line; 95% confidence interval shown). **f**, Approximately 1 in 4 MIN6 β-cells  
767 possess highly concentrated GLP1R clusters (Bar graph shows mean ± SEM) (n = 3 images,  
768 15 cells). **g**, Single molecule microscopy and tracking of **LUXendin645**- and **LUXendin651**-  
769 labeled GLP1R (n = 2 movies) (scale bar = 3 μm). **h**, Mean square displacement (MSD)  
770 analysis showing different GLP1R diffusion modes (representative trajectories are displayed)  
771 (scale bar = 1 μm).

772

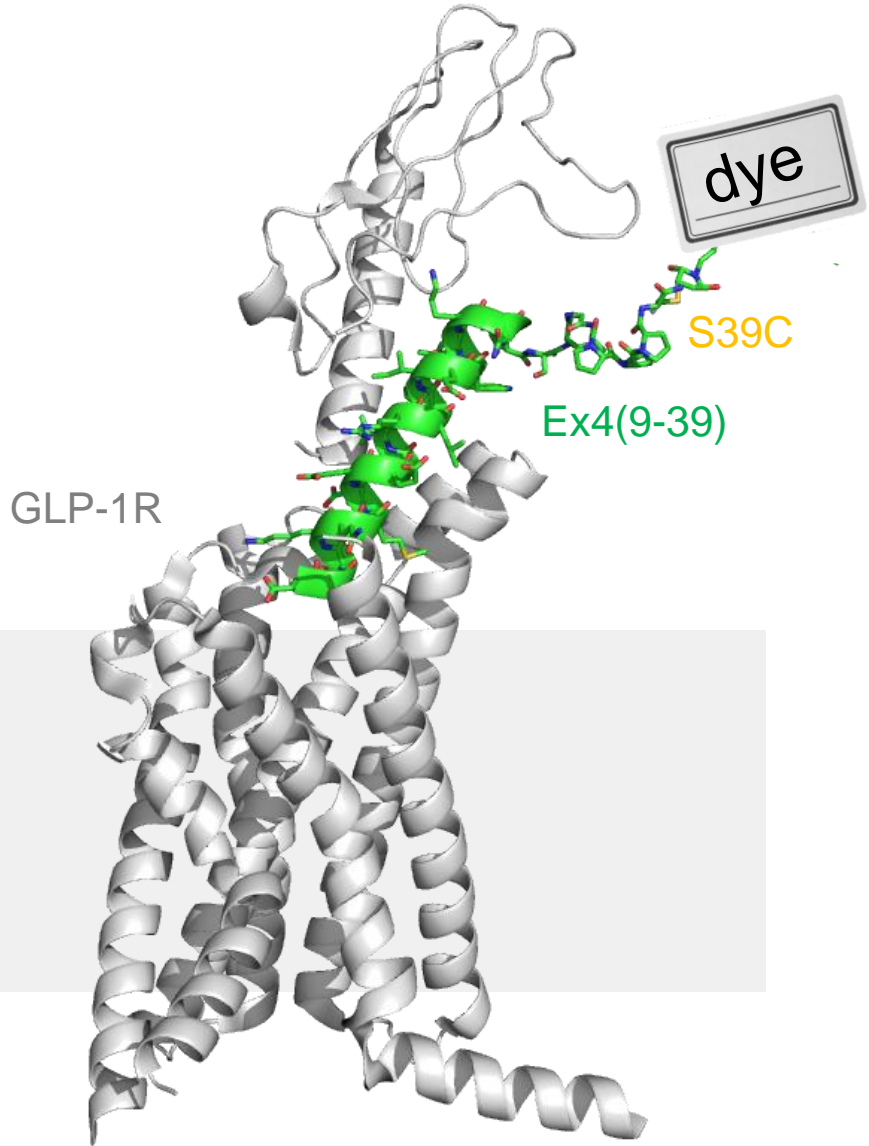
773 **Figure 6: LUXendin555 displays agonist properties and allows *in vivo* labeling of**  
774 **islets. a and b, LUXendin555 labels YFP-AD293\_SNAP-GLP1R (a) but not YFP-AD293 (b)**  
775 **controls (n = 3–4 assays) (10x scale bar = 213  $\mu$ m; 100x scale bar = 21  $\mu$ m). c, High**  
776 **resolution snapshot of LUXendin555-labeling in MIN6  $\beta$ -cells showing a punctate staining**  
777 **pattern in the cytosol (n = 8 images, 142 cells) (scale bar = 9  $\mu$ m). d, Surface GLP1R**  
778 **expression is reduced in LUXendin555- compared to LUXendin645-treated islets**  
779 **(representative images shown above each bar) (n = 5 islets; Student's unpaired t-test) (Bar**  
780 **graph shows mean  $\pm$  SEM) (scale bar = 17  $\mu$ m). e, LUXendin555 potently increases cAMP**  
781 **levels in YFP-AD293\_SNAP-GLP1R but not YFP-AD293 cells (n = 3 assays). f, Allosteric**  
782 **modulation with BETP increases agonist activity of LUXendin555 (n = 3 assays). g,**  
783 **Schematic depicting the two-photon imaging set up for visualization of the intact pancreas in**  
784 **mice. h, Representative image showing that LUXendin555 labels cell membranes in an**  
785 **islet surrounded by the vasculature *in vivo* (n = 2 islets from 1 mouse) (scale bar = 50  $\mu$ m).**  
786 **Mean  $\pm$  SE are shown. \*\*P<0.01.**

787

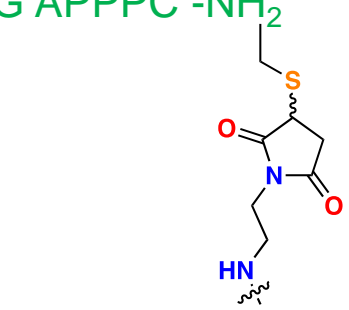
10 15 20 25 30 35

Exendin4(9-39) H<sub>2</sub>N- D LSKQM EEEAV RLFIE WLKNG GPSSG APPPS -NH<sub>2</sub>

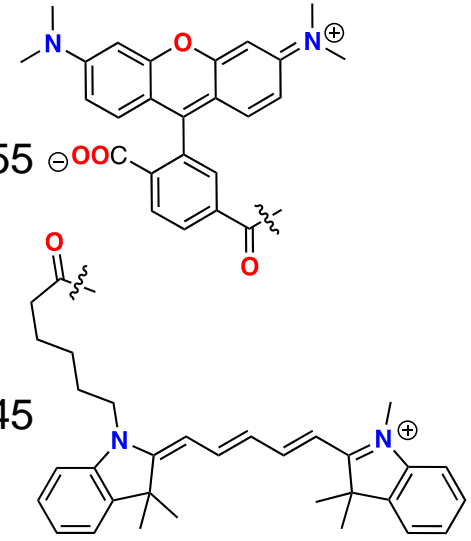
S39C-Ex4(9-39) H<sub>2</sub>N- D LSKQM EEEAV RLFIE WLKNG GPSSG APPPC -NH<sub>2</sub>



LUXendin555



LUXendin645



LUXendin651

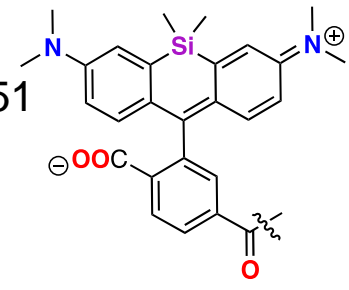


Figure 2

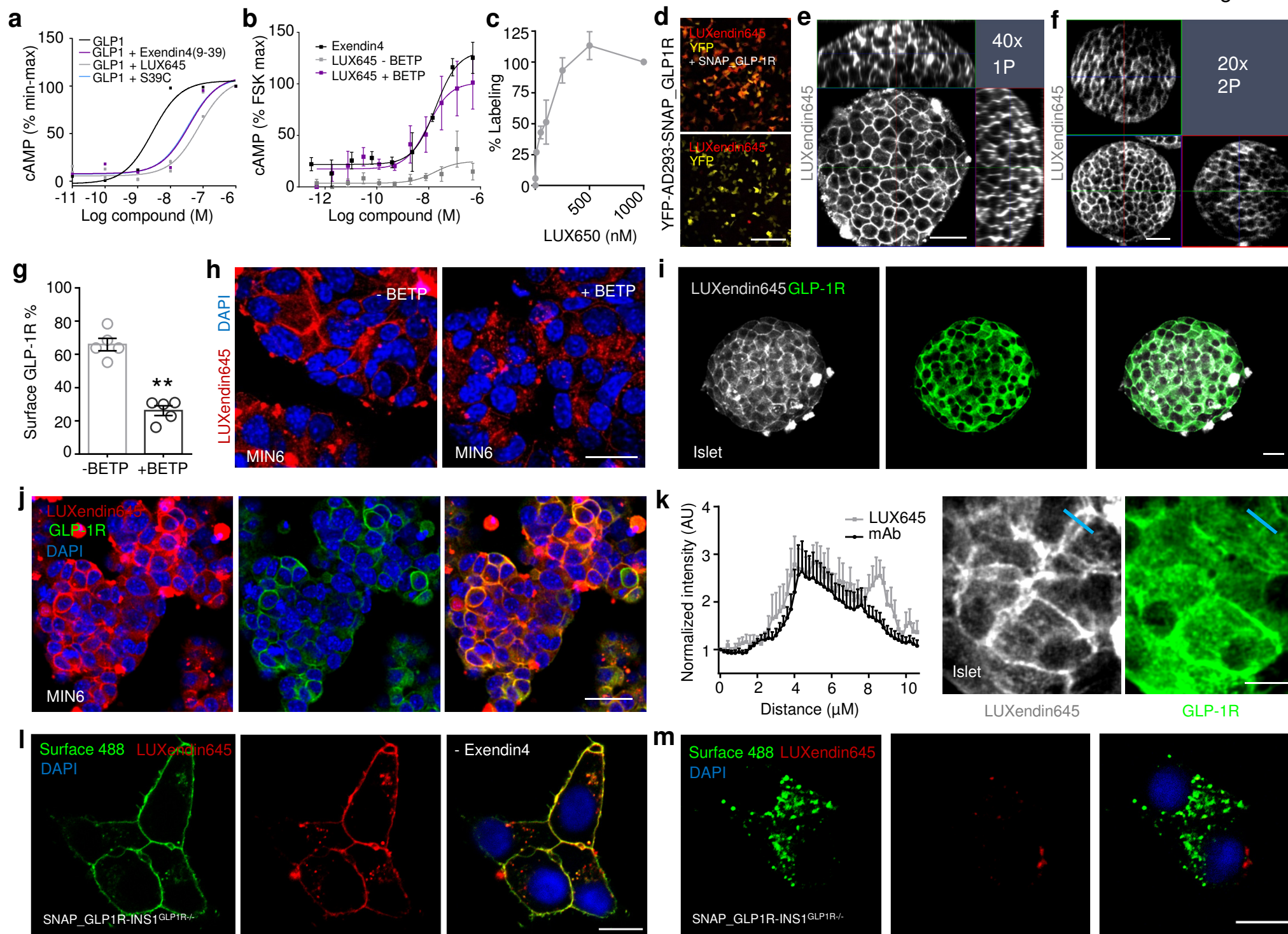


Figure 3

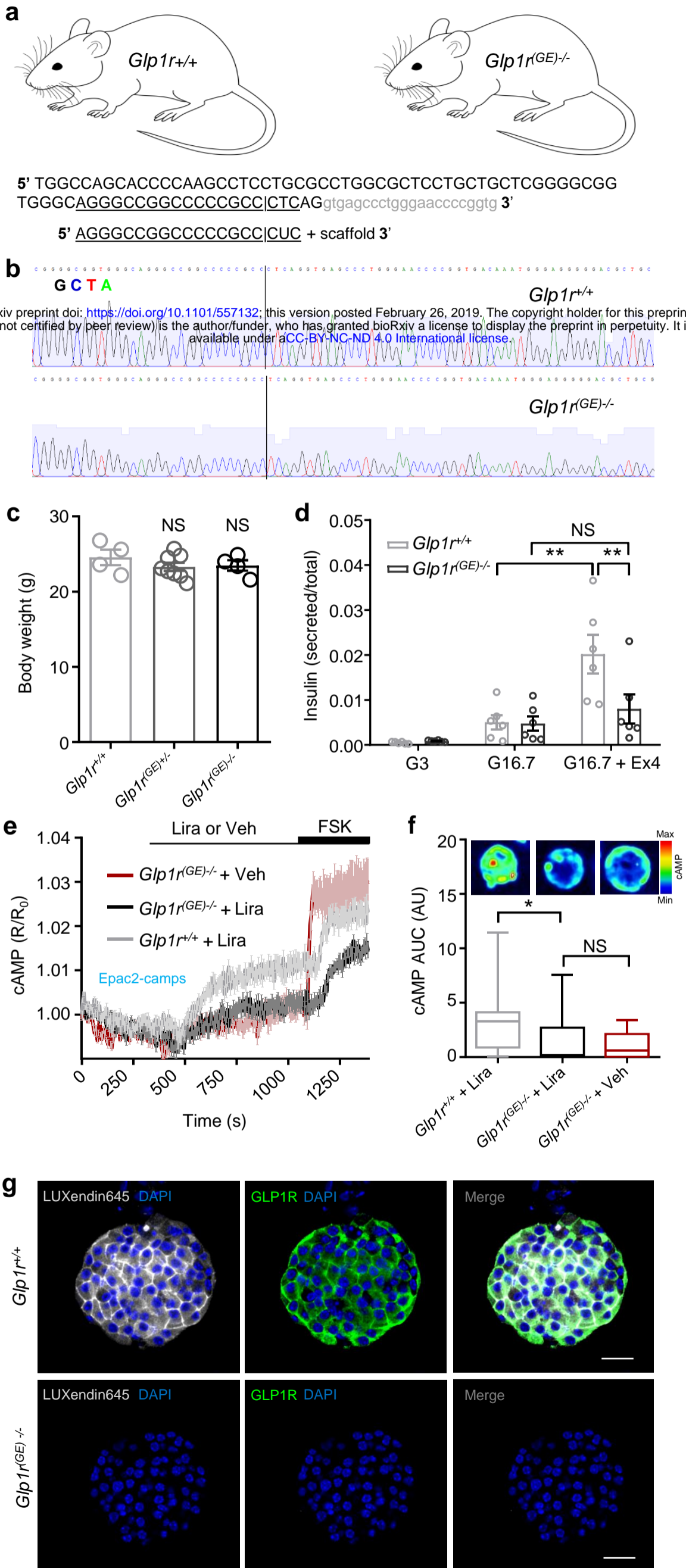
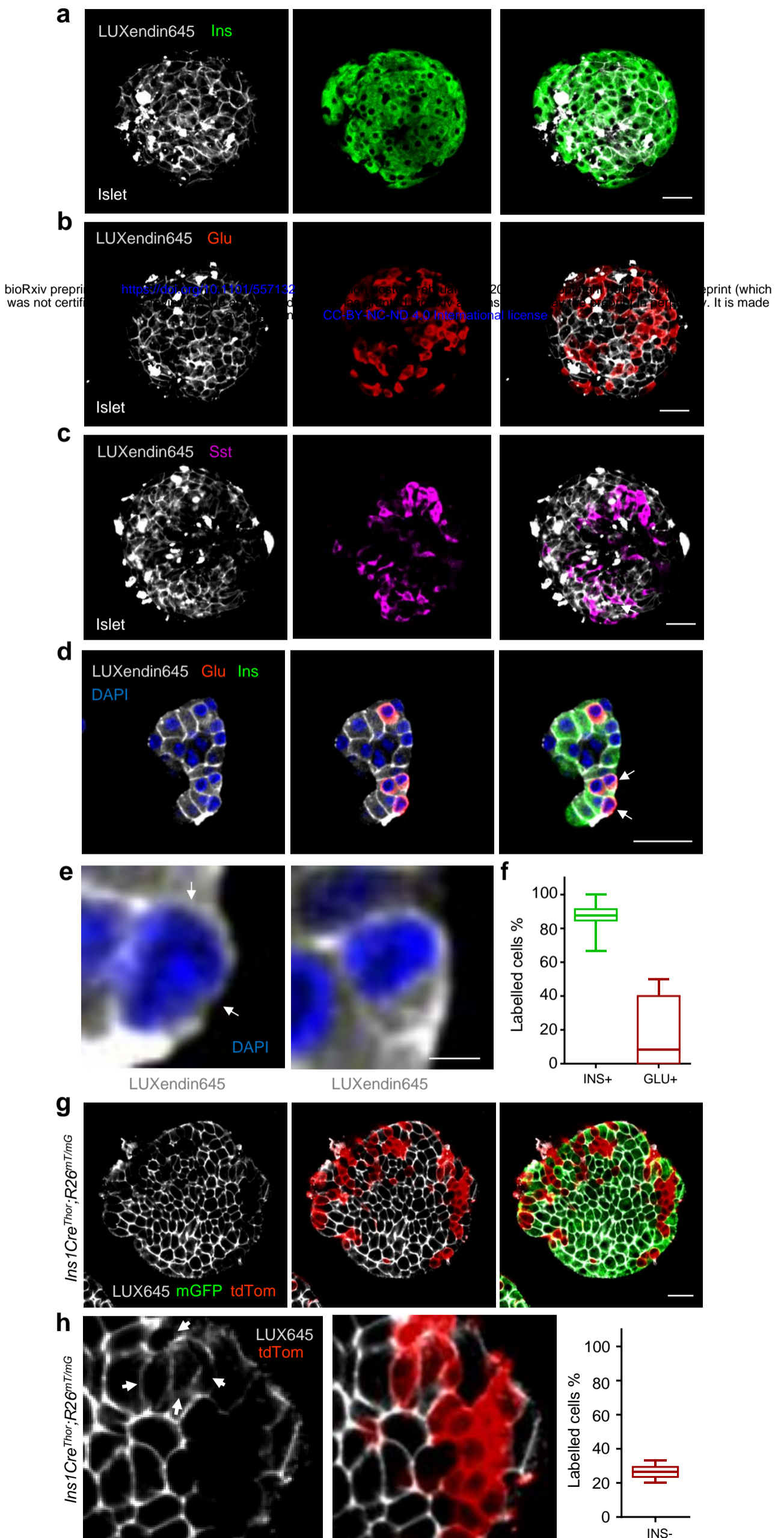




Figure 4



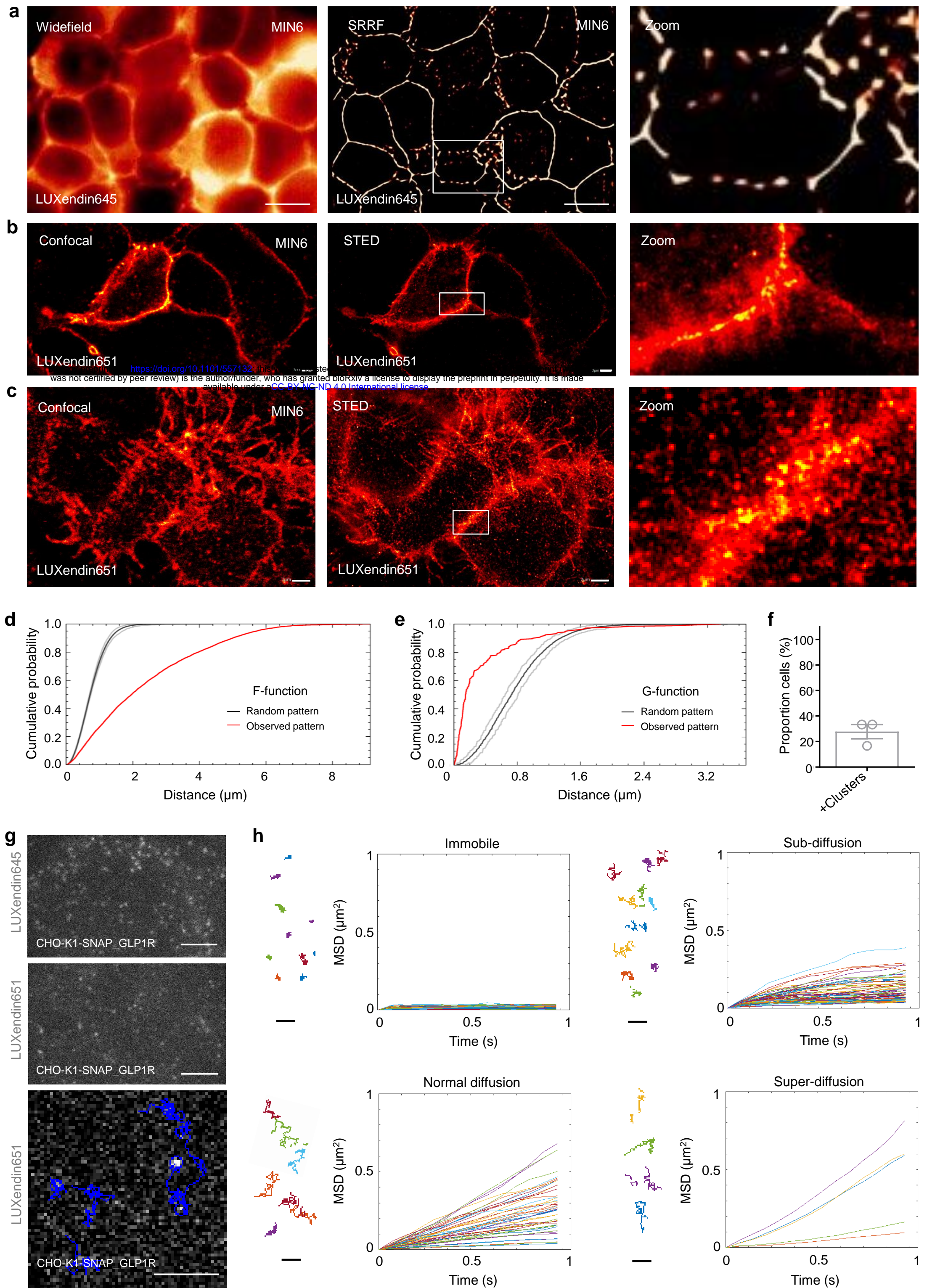


Figure 6

